Nigerian Research Journal of Chemical Sciences (ISSN: 2682-6054)
Volume 14, Issue 1, 2026

Assessment of Dye Sensitized Solar Cell with an Organic Photosensitizer Featuring Orderly Conjugated Benzo(D)Thiazol2amine

*Bakare M.A., Obadahun J., Agho O.B., Enyeribe C.C., Onikosi B.O., Hassan S.I., Usman N.D, Aliyu A.S. and Abusufyan Y.

Department of Science Laboratory Technology,

Nigerian Institute of Leather and Science Technology (NILEST),

Samaru, Zaria. Kaduna State, Nigeria.

* Corresponding Author: muhammedabbasbakare@gmail.com

Accepted: *January 3, 2026.* **Published Online***: January 14, 2026*

ABSTRACT

The aim of this study was to synthesize and characterize two benzothiazole–azo derivatives (Dye A1 and Dye A2) to evaluate their structural, optical, and photovoltaic properties. The dyes were prepared through diazo coupling reactions and characterized using physical measurements, UV–Visible spectroscopy, FT-IR spectroscopy, and photoelectrochemical analysis of dye-sensitized solar cells (DSSCs). Physical characterization revealed melting points ranging from 184–202 °C, with Dye A1 obtained as a dark red solid and Dye A2 as a brown solid. UV–Visible spectroscopy showed absorption maxima at 444 nm for Dye A1 and 540 nm for Dye A2, with molar absorptivity values of 24,809 $L \cdot mol^{-1} \cdot cm^{-1}$ and 7,009 $L \cdot mol^{-1} \cdot cm^{-1}$ respectively, confirming differences in conjugation and electronic transition probability. FT-IR spectra verified the presence of characteristic functional groups including C=O, N–H, C–H, and azo –N=N– linkages. Photovoltaic testing demonstrated that DSSCs sensitized with Dye A1 achieved a conversion efficiency of 1.45%, while Dye A2 recorded a slightly higher efficiency of 1.69%, attributed to improved photocurrent and fill factor. These findings highlight the potential of benzothiazole–azo chromophores as effective organic sensitizers for DSSCs.

Keywords: Conversion efficiency, Fill factor, Molar absorptivity, Open-circuit voltage, Short-circuit current density, UV–Visible spectroscopy

INTRODUCTION

Solar energy is a good candidate for renewable energy. The energy provided by the sun in one hour is larger than the energy consumption globally in an entire year [1]. However, capturing solar

energy and converting it to chemical or electrical energy at low cost is still a big challenge. Photovoltaic cells are one of the devices used to capture solar energy, and crystalline silicon-based photovoltaic devices are the most widely used at present, with solar-to-electricity conversion efficiencies above 20% for multicrystalline silicon solar cells [2]. They are now at a mature state of technical development, but the high cost of manufacturing restricts their competition with traditional energy sources.

There are various types of solar cells; Crystalline silicon solar cells dominate the market at present. To meet the demand of reducing material and purification costs, thin-film solar cells have been developed [3]. Thin-film solar cells are based on thin layers of semiconductor materials such as amorphous silicon, cadmium telluride (CdTe), and copper indium gallium diselenide (CIGS). Even though thin-film solar cells require less material, the complex production processes involving rare materials are expensive and may limit future large-scale production [4].

During the past two decades, tremendous efforts have been focused on the development of photovoltaic (PV) technologies capable of addressing some drawbacks of conventional silicon-based solar panels, such as heaviness, opaqueness, and large energy consumption during manufacturing [5]. Technologies integrating organic and hybrid materials such as Dye-Sensitized Solar Cells (DSSCs), Bulk-Heterojunction solar cells (BHJ), and Perovskite Solar Cells (PSC) have progressed significantly [6]. Nowadays, these technologies appear adapted to solve some of these drawbacks. In terms of power conversion efficiencies (PCEs), the best DSSC performances lie in the range of 10–14.2% [7], which is lower compared to BHJ and PSC, but DSSCs have already demonstrated superior long-term stability. When non-volatile electrolytes are employed, their performance can be conserved under harsh testing conditions [8], and stability corresponding to approximately 10 years of use in real conditions has been demonstrated. Furthermore, this technology enables the fabrication of semi-transparent solar panels that can be colorful and prepared with non-toxic constituents [9]. All these criteria make DSSCs very appealing for Building-Integrated Photovoltaics (BIPV) [10] or Automobile-Integrated Photovoltaics (AIPV) [11]. The performance of a DSSC mainly depends on the molecular structure of the dye used to photosensitize the mesoporous electrode.

The demand for renewable energy sources has driven significant research into solar energy conversion technologies, particularly Dye-Sensitized Solar Cells (DSSCs), due to their low-cost fabrication, flexibility, and high theoretical efficiency [12]. However, efficiency and stability

remain major challenges, especially with conventional metal-based photosensitizers like ruthenium complexes, which suffer from high costs, carcinogenicity, scarcity, and environmental concerns [13].

The global energy crisis and environmental concerns have intensified the search for efficient, cost-effective, and sustainable photovoltaic technologies. DSSCs have emerged as a promising alternative to conventional silicon-based solar cells due to their low production costs, lightweight nature, and ability to perform efficiently under low-light conditions [12]. Despite these advantages, DSSCs still face critical challenges, particularly regarding efficiency, long-term stability, and the environmental impact of traditional photosensitizers [14]. Organic photosensitizers have emerged as promising alternatives due to their tunable optical properties, high molar extinction coefficients, and environmentally friendly nature [14]. Among various organic dyes, benzo[d]thiazol-2-amine derivatives have shown great potential due to their extended conjugation, strong charge transfer capability, and excellent light-harvesting ability [15]. However, the relationship between molecular structure, electron injection efficiency, and long-term stability in DSSCs using orderly conjugated benzo[d]thiazol-2-amine remains underexplored.

This project centered on assessment of dye sensitized solar cell with an organic photosentizer featuring orderly conjugated benzo[d]thiazol-2-amine. The Aim was achieved through the following objectives;

i. Synthesis of dye-sensitizer from benzo[d]thiazol-2-amine.
ii. Characterization of the dye-sentizer's via UV-visible, FT-IR spectroscopy and Fabrication of the cells using the dye-sensitizes as the light absorber.
iii. Photovoltaic property assessment of the cell such as open circuilt voltage (V_{OC}), close circuit current density (Jsc) and percentage solar efficiency

MATERIALS AND METHODS

Materials

Analytical grade reagents and chemicals from sigma Aldrich was used for this research work These include; N,N-dimethylbenzo-1,4-diamine, Ammoniumthiocyanates, 3-amino-2-methylbenzoic acid, DMF,Sodium nitrite.Other materials used are: Magnetic stirrer, oven, reflux condenser, Agilent CARY 300 UV- visible spectrophotometer.

Synthesis of 1, 3-benzothiazole-2, 6-diamine (Intermediate)

N,N-dimethylbenzo-1,4-diamine (4.6 g, 0.05 mol) and ammonium thiocyanate (3.8 g, 0.05 mol) were both weighed separately and dissolved in absolute ethanol (15 ml) containing 4 ml of Conc HCl. Bromine (2.0 ml) in glacial acetic acid (6.75 ml) was added to this mixture, and the reaction mixture was refluxed for 1 hour and then cooled in an ice bath. The obtained precipitate was filtered, rinsed with cold water, and dried and the product was re-crystallized from ethanol.

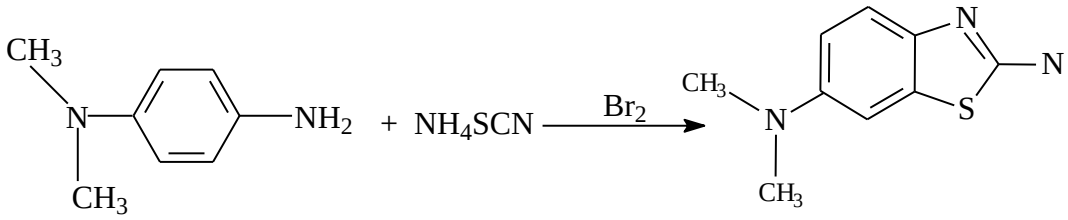

N, N-dimethylbenzo-1,4-diamine 2-aminobenzothiazole

Scheme 1: Synthesis of 1, 3-benzothiazole-2, 6-diamine (Intermediate)

Diazotizations of 2-aminobenzothiazole Intermediates

A solution of 2-aminobenzothiazole (0.054 mole) in H_2SO_4 (12 ml) was cooled to 0- 4 °C. To this solution was added a cold solution of sodium nitrite (0.54 mole) drop wise with constant stirring. When the addition was complete, the resultant reaction mixture was left in ice-bath for 1hr. It was used as such for further reaction as shown in the reaction below:

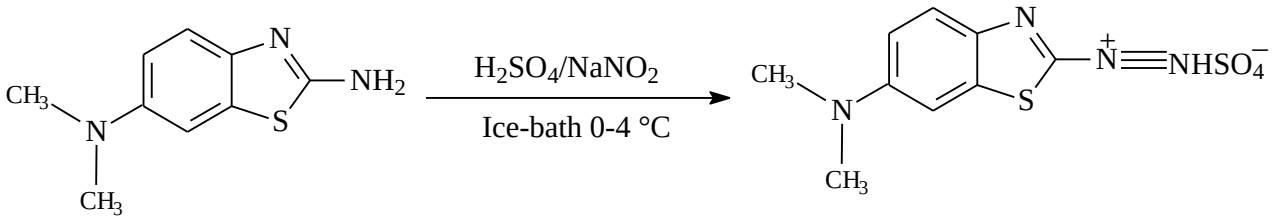

2-aminobenzothiazole diazonium salt of 2-aminobenzothiazole

Scheme 2: Diazotizations of the 2-aminobenzothiazole Intermediates

Coupling Reaction

Separately, the coupling components of 3-amino-2-methylbenzoic acid and 3,5-dimethylbenzoic acid were dissolved in DMF and cooled to 0 °C by the addition of ice. The intermediate obtained from 2-aminobenzothiazole diazonium solutions was then added dropwise over 30–40 minutes with vigorous stirring [16]. The mixture was further agitated for 3 hours at 5 °C before the pH of

the solution was adjusted to 4–5 using 5 ml of 10% NaOH. The finished product was subsequently filtered, rinsed with cold water, and dried. The crude product was purified by recrystallization from a 9:1 mixture of ethanol and DMF.

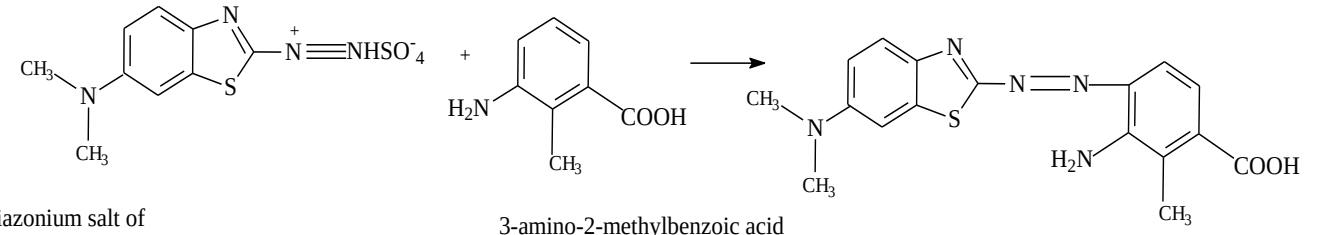

Diazonium salt of *N,N*-dimethyl-2,3-dihydro-1,3-benzothiazol-6-amine

3-amino-2-methylbenzoic acid

3-amino-2-methyl-5-[(4-(N,N-dimethyl-2,3 -dihydro-1,3-benz0thiazol-6-yl)azo)]benzoic acid

Scheme 3: Coupling Reaction of the diazonium salt with 3-amino-2-methylbenzoic acid

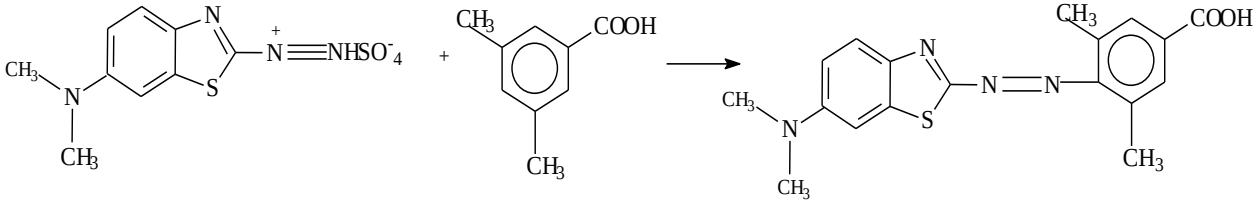

Diazonium salt of *N,N*-dimethyl-2,3-dihydro-1,3-benzothiazol-6-amine

3,5-dimethylbenzoic acid

4-[(4-(*N,N*-dimethyl-2,3-dihydro-1,3 -benzothiazol-6-yl)diazenyl]-3,5-dimethylbenzoic acid

Scheme 4: Coupling Reaction of *N,N*-dimethly-2,3-dihydro-1,3-benzothiazol-6 amine with 3,5-dimethylbenzoic acid

Purification of the Dyes

A known weight of each dye was dissolved in a small amount of ethanol and heated. The solution was then filtered while still hot using a Buchner funnel and a suction pump. However, dyes obtained from intermediates 1 and 4 required a 9:1 solvent mixture of ethanol and DMF, as recommended by Alaa and Tarek [17].

Characterizataion of the Synthesized Dyes

The physicochemical properties and spectroscopic propertices of synthesized dyes and the azo dyes were carried out.

UV-Visible Spectroscopy

The dye sample was prepared by dissolving a known concentration of the compound in absolute ethanol. Pure ethanol was first used as a blank to calibrate the Agilent CARY 300 UV-Visible spectrophotometer and establish a baseline. The prepared dye solution was transferred into a clean quartz cuvette, which was placed in the sample holder of the instrument. The absorption spectrum

was recorded over the wavelength range of 200–800 nm. The obtained spectral data were analyzed to determine the absorption maxima (λmax), corresponding to electronic transitions within the dye molecules, thereby providing information on conjugation and chromophoric properties [18].

FT-IR Spectroscopy

The dye sample was prepared according to its physical state. Solid samples were finely ground and mixed with potassium bromide (KBr) to form pellets, while liquid or powdered samples were analyzed directly using the ATR accessory. A background spectrum was first recorded to eliminate interference from atmospheric water vapor and carbon dioxide. The prepared sample was then placed on the ATR crystal of the Agilent CARY 630 FT-IR spectrophotometer, and the infrared spectrum was recorded over the range of 4000–400 cm^{-1}. The resulting spectra were analyzed to identify characteristic absorption bands corresponding to functional groups present in the intermediates and synthesized dyes, thereby confirming structural modifications during the synthesis process [18].

TiO_2 Electrode Preparation and Device Preparation

DSSC was fabricated using photoelectrode layer, spacer, and counter electrode placed on a single FTO substrate. [19], photo-anodes made of nano-crystalline TiO_2 and a counter electrode was prepared. Fluorene doped tin oxide (FTO) coated glass (2.2 mm thickness, sheet resistance of 8/cm2, TEC Pilkington) was washed in the following order: detergent, water, acetone, and ethanol. Following this, the FTO glass plates was submerged in a 40 mM aqueous $TiCl_4$ solution at 70 °C for 30 minutes before being rinsed with water and ethanol. Screen printing was used to deposit a thin coating of TiO_2 (Solaronix, Ti-Nanoxide D/SP) (active area, 1.0 cm2) on clear conducting glass. After 6 minutes of drying at 120 °C, scattering layer TiO_2 particles (Solaronix, Ti-Nanoxide D/SP) was printed. The TiO_2 electrodes was heated in an air flow at 350 °C for 10 minutes, then at 500 °C for 30 minutes. The ZrO_2 paste was prepared according to a the manufacturer procedure using ZrO_2 nanoparticles (40–50 nm; Fulka, USA). The substrate was heated on the hotplate at 200 °C for 1 h. When the substrate cooled, carbon paste was printed on the ZrO_2 layer to form a layer with thickness of 130 μm. At the same time, the carbon layer was connected to the other FTO layer and sintered at 400 °C (Figure 1).The dye-coated electrodes was rinsed with acetonitrile and combined with glass plates by heating a hot-melt glue film at 250 °C for 1 min (150 μm thick; Bynel 4164, DuPont, USA). A drop of the electrolyte solution was placed into a hole drilled into

the glass of the assembled cell and driven into the cell by vacuum backfilling. Finally, the hole was sealed using additional Bynel film and a glass cover slip (0.1 mm thick). The electrolyte was composed of 0.2 M I_2, 0.5 M *N*-methylbenzimidazole, and 0.1 M guanidinium thiocyanate in acetonitrile and valeronitrile solution (1 : 1 v/v), which has been used in highly durability DSSCs. shown in the figure below:

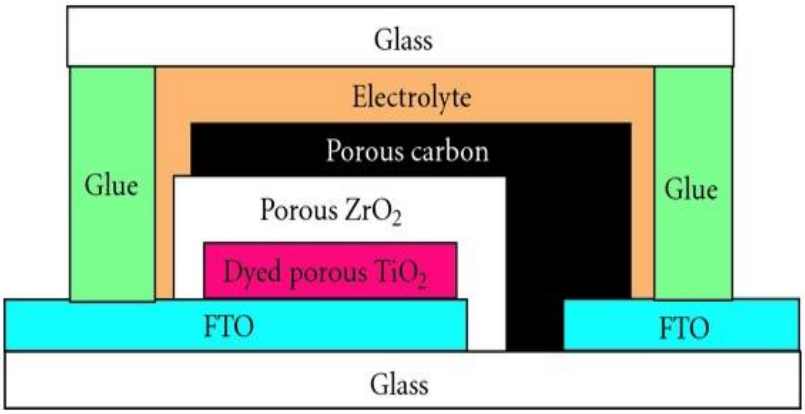

Figure 1: Fabrication of dye sensitized solar cell

Photo-Electrochemical Measurement

Photocurrent-voltage characteristics of DSSCs was measured using a Keithly 2400 source meter under illumination of AM 1.5 G solar light from solar simulator (SOL3 A, Oriel) equipped with a 450 W xenon lamp (91160. Oriel). The incident light intensity was calibrated using a reference Si solar cell (Newport Oriel.91150 V) to set 1 Sun (100 mW/cm^2) and the J-V curve was generated to obtaine the cell performance parameters, including short-circuit current (J_{sc}), open circuit voltage (V_{oc}), maximum power (V_{max}), (J_{max}), fill factor (ff) and overall cell conversion efficiency, was measured and calculated from each J-V characteristic curve [20].

RESULTS AND DISCUSSION

Table 1 shows the basic physical properties of dyes A1 and A2, including molecular weight, yield, melting point, and colour. Dye A1 was obtained as a dark red solid with higher thermal stability but slightly lower yield, while Dye A2 appeared brown with a higher yield but reduced melting point due to steric hindrance from methyl substituents.

Table 1: Physical Properties of the Synthesized dyes

Dye No.	Molecular Formula	Molecular Weight (g/mol)	Colour of the Dye	% Yield	Melting point ^{o}C
A1	$C_{17}H_{17}O_2N_5S$	355.43	Dark red	80	200-202
A2	$C_{16}H_{16}O_2N_6S$	356.418	Brown	87	184-186

NOTE:

A1: 3-amino-2-methyl-5-[(4-(*N*,*N*-dimethyl-2,3-dihydro-1,3-benzothiazol-6-yl)azo]benzoic acid.

A2: 4-[(4-(*N*,*N*-dimethyl-2,3-dihydro-1,3-benzothiazol-6-yl]-3,5-dimethylbenzoic acid.

Physical Properties of the Synthesized Dyes

The molecular formula, molecular weight, melting point, percentage yield, and appearance of the dye crystals the synthezed dye were presented in Table 1. above. Dye A1 with the molecular mass 355.43 g/mol was obtained as a dark red crystalline solid in 80 % yield with a melting point of 200–202 °C. The relatively high melting point is indicative of strong intermolecular forces, particularly hydrogen bonding through the carboxylic acid group and π–π stacking interactions across the aromatic and azo moieties. These stabilizing forces enhance the crystal lattice cohesion, accounting for the higher thermal stability of dye A1. The deep red coloration suggests an extended conjugation pathway and efficient resonance delocalization within the chromophore system. Previous studies have shown that azo dyes with fewer steric disturbances and stronger resonance stabilization display higher melting points and bathochromic shifts toward red coloration [21,22]. Dye A2 356.42 g/mol, on the other hand, appeared brown and was isolated in a slightly higher yield of 87% but with a lower melting point of 184–186 °C. The reduced melting point can be attributed to steric hindrance introduced by the additional 3,5dimethyl substituents, which disrupt planarity and limit efficient intermolecular hydrogen bonding. This steric effect weakens lattice packing and reduces thermal stability, a trend commonly observed in methyl-substituted azo dyes [23]. The brown coloration of dye A2 may also be as a result of slight distortion in the conjugated system, which restricts electron delocalization across the azo linkage, thus shifting absorption toward shorter wavelengths and reducing color intensity. This observation aligns with earlier reports showing that electron donating substituents, while enhancing reactivity, can also compromise planarity and affect optical properties [22,24]..Interestingly, the yield of dye A2 was

slightly higher than that of dye A1. This may be due to the electron-donating nature of the methyl substituents, which increase electron density on the coupling ring, thereby improving the nucleophilicity of the reactive center during diazo coupling. Similar observations were reported by Karakaya *et al.* [25], who found that electron-donating groups enhanced coupling efficiency under aqueous conditions. Although the methyl groups reduce thermal stability, they appear to facilitate a smoother reaction pathway, accounting for the higher synthetic yield. Taken together, these findings demonstrate how small structural modifications profoundly influence azo dye properties. Dye A1, though obtained in slightly lower yield, offers better thermal stability and deeper coloration due to efficient intermolecular interactions and resonance stabilization. Conversely, dye A2 provides higher synthetic efficiency but at the expense of color depth and melting point stability. This structure–property relationship is consistent with earlier reports on azo dye chemistry, where substituent effects significantly modulate melting behavior, yield, and chromophoric absorption [21,23,25].

Table 2 and Figures 2 and 3 present the FT-IR spectra of dyes A1 and A2, confirming the presence of carbonyl, C–H, N–H, and azo (N=N) functional groups. Both dyes showed strong carbonyl and amine absorptions, while the azo bands differed slightly, reflecting structural variations that influence conjugation and bond localization.

Table 2: FT-IR Absorption Frequency of the Dyes

Dye No.	C=O Stretch (cm^{-1})	C-H Stretch (cm^{-1})	N-H Stretch (cm^{-1})	N=N Stretch (cm^{-1})
A1	1707.42, 1741.37, 1648.28	2840.56	3420.38	1592.2
A2	1707.55, 1745.57	2840.74	3486.39	1503.45

NOTE:

A1: 3-amino-2-methyl-5-[(4-(*N*,*N*-dimethyl-2,3-dihydro-1,3-benzothiazol-6-yl)azo]benzoic acid.

A2: 4-[(4-(*N*,*N*-dimethyl-2,3-dihydro-1,3-benzothiazol-6-yl]-3,5-dimethylbenzoic acid.

The Infra-Red Spectra of the Dyes

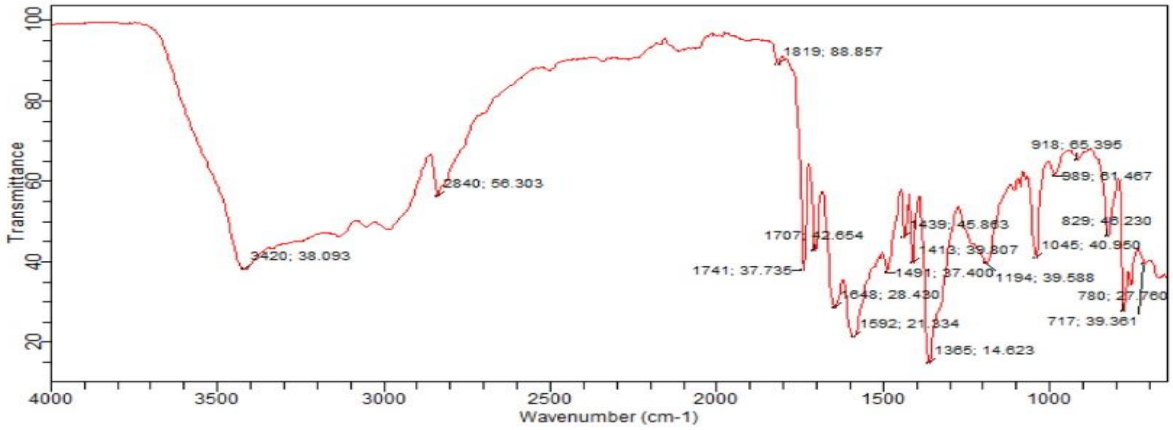

Figure 2: FT-IR DYE 1 SAMPLE

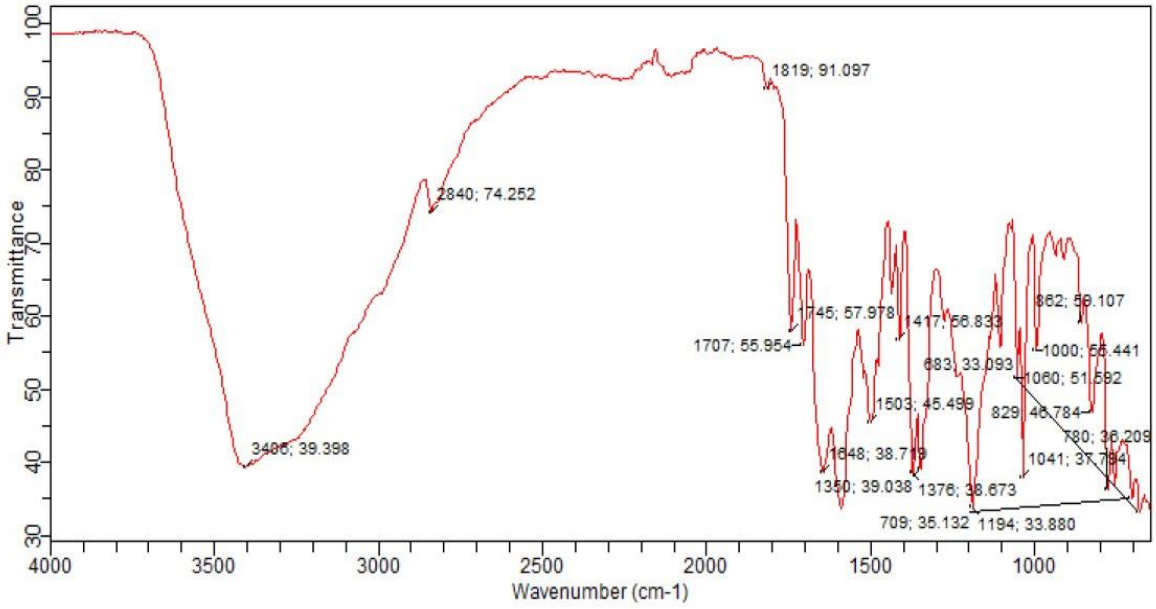

Figure 3: FT-IR DYE 2 PROCCESSED SAMPLE

The results of the infrared analysis carried out for the synthesized dyes are presented in Table 2. The FT-IR spectra revealed characteristic absorption bands corresponding to key functional groups that confirm their structural features. For Dye 1, notable peaks were observed at 1707.42, 1741.37, and 1648.28 cm^{-1}, which are attributable to carbonyl (C=O) stretching vibrations. These values fall within the expected region of 1650–1750 cm^{-1} and suggest the presence of both conjugated and non-conjugated carbonyl functionalities, as conjugation with aromatic systems typically shifts the stretching band to lower frequencies by approximately 20–30 cm^{-1} [26]. Similarly, Dye 2

exhibited strong C=O peaks at 1707.55 and 1745.57 cm^{-1}, reinforcing the presence of carbonyl groups in varied electronic environments.

Both dyes displayed C–H stretching vibrations at ~2840 cm^{-1}, characteristic of aliphatic hydrocarbons. Additionally, broad absorptions were recorded in the 3420–3486 cm^{-1} region, corresponding to N–H stretching vibrations. These absorptions are consistent with primary or secondary amines, and their broadness indicates possible hydrogen bonding, which is common in dye molecules containing auxochromic groups that enhance solubility and stability [27].

The azo functional group (–N=N–), a defining chromophore in many synthetic dyes, was confirmed by absorptions at 1592.20 cm^{-1} in Dye 1 and 1503.45 cm^{-1} in Dye 2. Azo linkages typically absorb in the 1400–1600 cm^{-1} range, with shifts depending on the extent of conjugation and substitution patterns on the aromatic rings [28]. The higher wavenumber of Dye 1's azo peak (1592 cm^{-1}) indicates a relatively more localized N=N bond, consistent with weaker conjugation in its aromatic system, while Dye 2's absorption is closer to the typical azo range, suggesting structural variation between the two dyes.

UV–Visible Absorption Analysis

Table 3, with Figures 4 and 5 highlight the UV–Vis absorption maxima and molar absorptivity of the dyes. Dye A1 absorbed at 444 nm with higher absorptivity, indicating stronger electronic transitions, while Dye A2 showed a bathochromic shift to 540 nm but lower absorptivity, suggesting extended conjugation but weaker transition probability.

Table 3: UV-Visible Spectroscopy of the Dyes

Dyes No	λ max (nm)	ε (L mol^{-1} cm^{-1})
A1	444	24,809
A2	540	7,0095

NOTE:

A1: 3-amino-2-methyl-5-[(4-(*N*,*N*-dimethyl-2,3-dihydro-1,3-benzothiazol-6-yl)azo]benzoic acid.

A2: 4-[(4-(*N*,*N*-dimethyl-2,3-dihydro-1,3-benzothiazol-6-yl]-3,5-dimethylbenzoic acid.

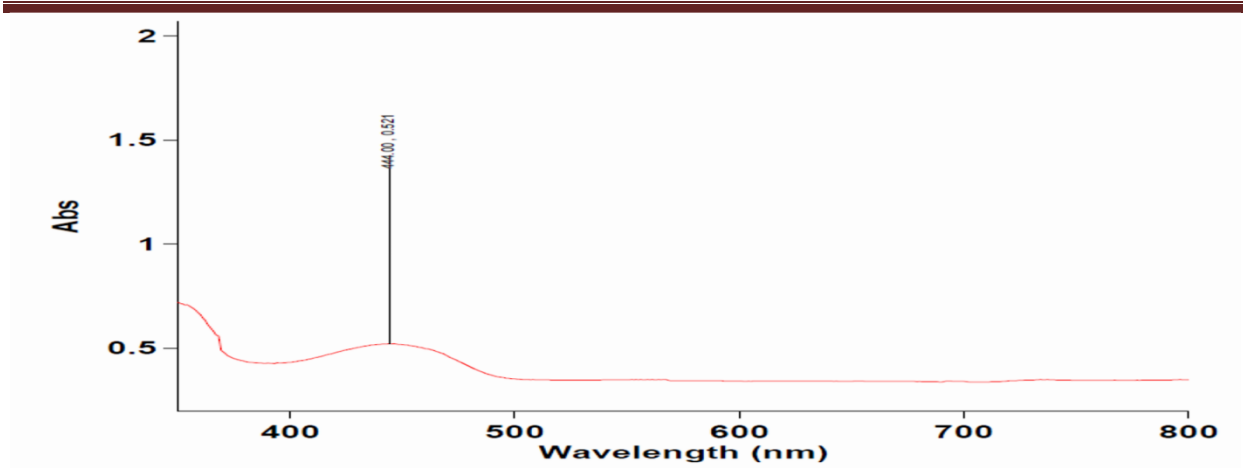

Figure 4: UV-Vis spectra for DYE 1 SAMPLE

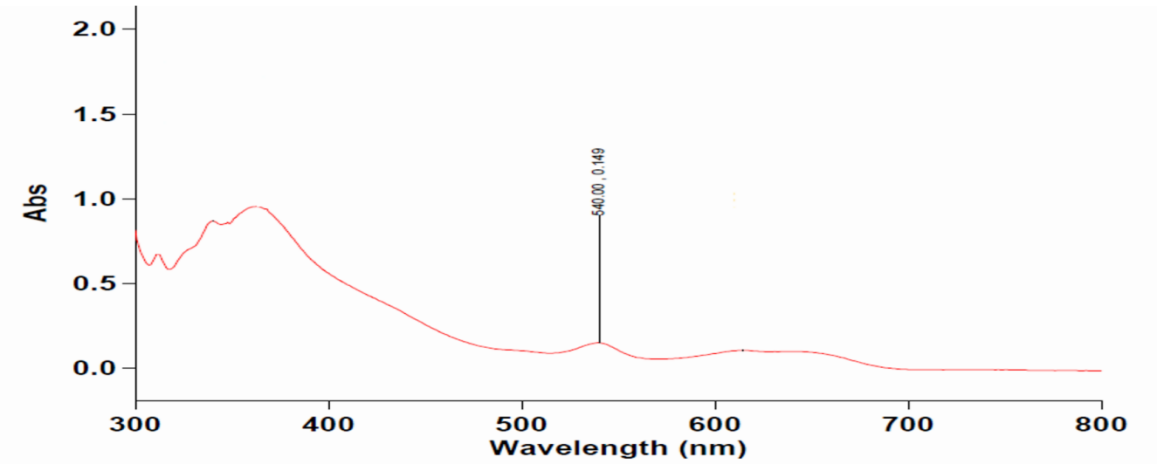

Figure 5: UV-Vis spectra for DYE 2 SAMPLE

The UV–Vis spectra of the synthesized dyes revealed distinct absorption maxima (λmax), which correspond to electronic transitions within the chromophoric systems. Dye 1 exhibited a λmax at 444 nm, while Dye 2 showed a red-shifted maximum at 540 nm. The bathochromic shift (red-shift) observed in Dye 2 indicates a more extended conjugation system or stronger electron-donating substituents compared to Dye 1. Such shifts are characteristic of azo dyes, where substitution patterns and auxochromic groups on the aromatic rings significantly influence the electronic transitions [29].

The molar absorptivity (ε) values further highlight the differences in chromophoric efficiency. Dye 1 recorded a higher absorptivity (ε = 24,809 L•mol^{-1}•cm^{-1}) compared to Dye 2 (ε = 7,009 L•mol^{-1}•cm^{-1}), suggesting that Dye 1 has stronger allowed electronic transitions, making it a more efficient absorber of visible light. The relatively low ε value of Dye 2 implies weaker

transition probability, which may be attributed to structural substitutions reducing orbital overlap or planarity of the chromophore [30].

The Current–Voltage (I–V) Characterization

Table 4 with Figures 5 and 7 compare the photovoltaic performance of DSSCs sensitized with dyes A1 and A2. Dye A1 achieved 1.012% efficiency, while Dye A2 performed better with 1.65% efficiency, due to higher Jsc and fill factor. This demonstrates that structural modifications, such as dimethyl substituents, can enhance light absorption and electron injection, improving solar cell efficiency.

Table 4: Photoelectrochemical Paramiters of the Cells Sensitized with Organic Dyes

Dye	V_{oc}(mV)	J_{sc}(mAcm^{-2})	FF	n%
A1	0.5	4.6	0.44	1.012
A2	0.5	5.7	0.58	1.65

NOTE:

A1: 3-amino-2-methyl-5-[(4-(*N*,*N*-dimethyl-2,3-dihydro-1,3-benzothiazol-6-yl)azo]benzoic acid.

A2: 4-[(4-(*N*,*N*-dimethyl-2,3-dihydro-1,3-benzothiazol-6-yl]-3,5-dimethylbenzoic acid.

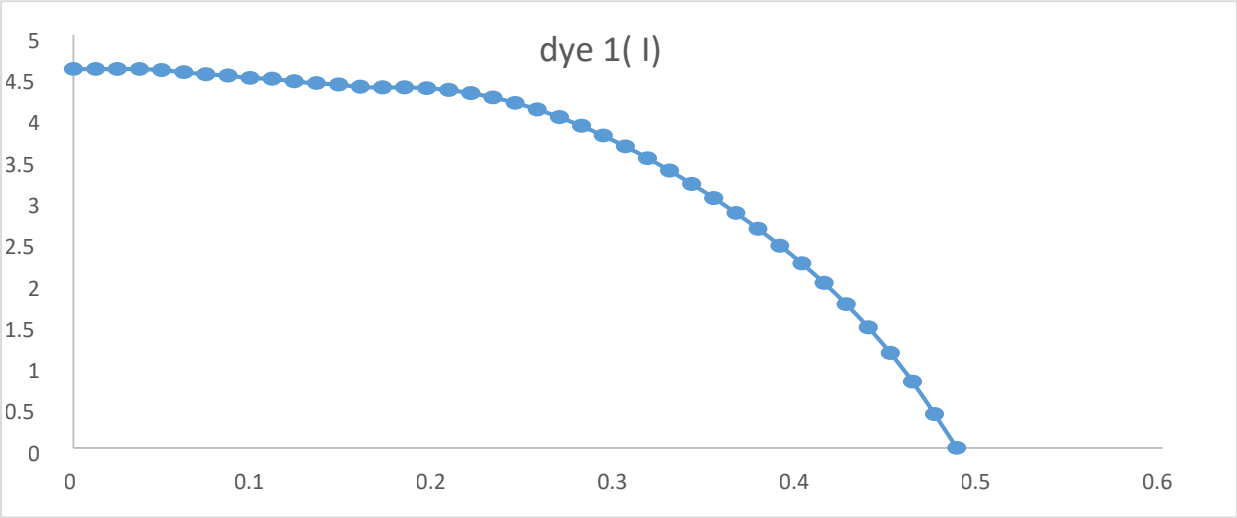

Figure 6: J-V curve Characteristic of the DSSC

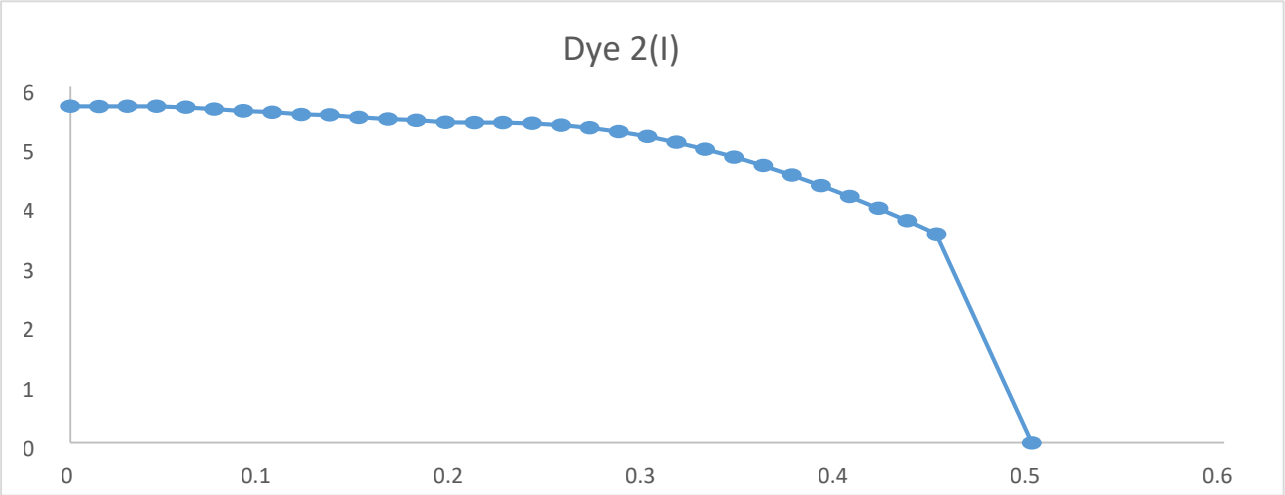

Figure 7: J-V curve Characteristic of the DSSC

The dye-sensitized solar cells (DSSCs) fabricated using the two synthesized dyes, 3-amino-2-methyl-5-[(4-(N,N-dimethyl-2,3-dihydro-1,3-benzothiazol-6-yl)azo]benzoic acid (Dye 1) and 4-[(4-(N,N-dimethyl-2,3-dihydro-1,3-benzothiazol-6-yl)]-3,5-dimethylbenzoic acid (Dye 2), were subjected to photoelectric characterization. The smooth I–V curves obtained are shown in Figures 6 and 7. Three key photovoltaic parameters were considered and compared: the short-circuit current density (Jsc), which corresponds to the highest current density; the open-circuit voltage (Voc), which is the maximum attainable voltage; and the fill factor (FF), which is a measure of the solar cell's quality and overall efficiency. From the calculations, the DSSC fabricated with Dye 1 exhibited a conversion efficiency of 1.45%, with an open-circuit voltage (Voc) of 0.50 V, short-circuit current density (Jsc) of 5.00 mA/cm², and fill factor (FF) of 0.58. In comparison, the DSSC fabricated with Dye 2 demonstrated a slightly higher performance, with a conversion efficiency of 1.69%, Voc of 0.50 V, Jsc of 5.66 mA/cm², and FF of 0.60. The higher Jsc and improved fill factor of Dye 2 indicate that the introduction of the dimethyl substituents on the benzoic acid ring enhanced light absorption and improved electron injection into the TiO_2 conduction band.

The results highlight the potential of these benzothiazole–azo derivatives as alternative photosensitizers. The performance of Dye 2, being slightly higher than Dye 1, suggests that structural modifications to the aromatic ring system can influence electron-donating ability and anchoring strength, thereby improving device efficiency. Previous studies have shown that

molecular tailoring of natural and synthetic dye structures can significantly affect photovoltaic parameters [31].

CONCLUSION

The present study highlights the successful synthesis, purification, and characterization of dyes A1 and A2, both obtained with high purity, as reflected in their yields of 80% and 87% and melting points of 200–202 °C and 184–186 °C, respectively. FT-IR analysis confirmed the presence of the expected functional groups, with A1 showing carbonyl absorptions at 1707–1741 cm^{-1}, an N–H stretch at 3420.38 cm^{-1}, and an azo band at 1592.2 cm^{-1}, while A2 exhibited similar carbonyl stretches at 1707–1745 cm^{-1}, an N–H band at 3486.39 cm^{-1}, and an -N=N- azo vibration at 1503.45 cm^{-1}. UV–Visible spectroscopy revealed distinct optical behaviors, with A1 absorbing at 444 nm and a molar absorptivity of 24,809 L mol^{-1} cm^{-1}, whereas A2 showed a red-shifted λmax at 540 nm and a significantly higher absorptivity of 70,095 L mol^{-1} cm^{-1}. These optical properties translated into superior DSSC performance for A2, which achieved higher short-circuit current density (5.7 mA cm^{-2}), fill factor (0.58), and energy conversion efficiency (1.65%) compared to A1 (4.6 mA cm^{-2}, 0.44, and 1.012%), while both maintained an open-circuit voltage of 0.50 V. Overall, the enhanced conjugation and substituent pattern in A2 significantly improved its light harvesting and photovoltaic efficiency, establishing it as a more effective dye for DSSC applications.

REFERENCES

[1] Caramori, S., Cristino, V., Boaretto, R., Argazzi, R., Bignozzi, C.A. & Di Carlo, A. (2010). New components for dye-sensitized solar cells. *International Journal of Photoenergy*, 2010, 1–16.

[2] Yamaguchi, M., Lee, K.-H., Araki, K., Kojima, N., & Ohshita, Y. (2018). Analysis for efficiency potential of crystalline Si solar cells. *Journal of Materials Research, 33*(18), 2621–2626. https://doi.org/10.1557/jmr.2018.262

[3] Marinado, T. (2009). Photoelectrochemical studies of dye-sensitized solar cells using organic dyes. Ph.D Thesis. Kungliga Tekniska Högskolan, Stockholm.

[4] Marinado, T. (2015). Photoelectrochemical studies of dye-sensitized solar cells using organic dyes. Ph.D Thesis. Kungliga Tekniska Högskolan, Stockholm.

[5] Hallam, B.J., Zhang, Y., Kim, M., Wang, L. & Verlinden, P. (2021). Design considerations for multi-terawatt scale manufacturing of existing and future photovoltaic technologies. *Energy & Environmental Science*, 14(11), 5587–5610.

[6] Lin, Y.-H., Sakai, N., Da, P., Wu, J., Sansom, H.C., Ramadan, A.J., Mahesh, S., Liu, J., Oliver, R.D.J., Lim, J., Aspitarte, L., Sharma, K., Madhu, P.K., Morales-Vilches, A.B., Nayak, P.K., Bai, S., Gao, F., Grovenor, C.R.M., Johnston, M.B., … Snaith, H.J. (2020). A piperidinium salt stabilizes efficient metal-halide perovskite solar cells. *Science*, 369(6499), 96–102.

[7] Mathew, S., Yella, A., Gao, P., Humphry-Baker, R., Curchod, B.F.E., Tavernelli, I., Rothlisberger, U., Nazeeruddin, M.K. & Grätzel, M. (2014). Dye-sensitized solar cells with 13% efficiency achieved through the molecular engineering of porphyrin sensitizers. *Nature Chemistry*, 6(3), 242–247.

[8] Joly, D., Pellejà, L., Narbey, S., Oswald, F., Chiron, J., Clifford, J.N., Palomares, E. & Demadrille, R. (2014). A robust organic dye for dye-sensitized solar cells based on iodine/iodide electrolytes combining high efficiency and outstanding stability. *Scientific Reports*, 4, 4033.

[9] Yuan, H., Wang, W., Xu, D., Xu, Q., Xie, J., Chen, X., Zhang, T., Xiong, C., He, Y., Zhang, Y., Liu, Y. & Shen, H. (2018). Outdoor testing and ageing of dye-sensitized solar cells for building-integrated photovoltaics. *Solar Energy*, 165, 233–239.

[10] Fakharuddin, A., Jose, R., Brown, T.M., Fabregat-Santiago, F. & Bisquert, J. (2014). A perspective on the production of dye-sensitized solar modules. *Energy & Environmental Science*, 7(12), 3952–3981.

[11] Nazeeruddin, M.K., Kay, A., Rodicio, I., Humphry-Baker, R., Müller, E., Liska, P., Vlachopoulos, N. & Grätzel, M. (1993). Conversion of light to electricity by cis-X_2bis(2,2′-bipyridyl-4,4′-dicarboxylate) ruthenium(II) charge-transfer sensitizers. *Journal of the American Chemical Society*, 115(14), 6382–6390.

[12] O'Regan, B. & Grätzel, M. (1991). A low-cost, high-efficiency solar cell based on dye-sensitized colloidal TiO_2 films. *Nature*, 353, 737–740.

[13] Chiba, Y., Islam, A., Watanabe, Y., Komiya, R., Koide, N. & Han, L.Y. (2006). Dye-sensitized solar cells with conversion efficiency of 11.1%. *Japanese Journal of Applied Physics*, 45(25), L638–L640.

[14] Wang, P., Zakeeruddin, S.M., Comte, P., Charvet, R., Humphry-Baker, R. & Grätzel, M. (2003). Enhance the performance of dye-sensitized solar cells by co-grafting amphiphilic ruthenium sensitizer and hydrophobic coadsorbent. *Journal of Physical Chemistry B,* 107(48), 14336–14341.

[15] Zhang, H., Li, Y., Wang, J. & Liu, X. (2020). Benzo[d]thiazol-2-amine derivatives for DSSCs: Synthesis and characterization. *Journal of Molecular Structure*, 1200, 127–135.

[16] Maradiya, H.R. & Patel, V.S. (2010). Synthesis and dyeing performance of some novel thiazole azo disperse dyes. *Journal of Saudi Chemical Society*, 14(1), 77–81.

[17] Alaa, H. & Tarek, A. (2006). Purification methods for azo dyes. *Pigment & Resin Technology*, 35(2), 112–118.

[18] Nasir, V., Yakubu, M.K., Bello, K.A. & Obinna-Nkeonye, P. (2021). Synthesis and dyeing performance of some amphiphilic naphthalimide azo disperse dyes on polyester fabrics. *Journal of the Serbian Chemical Society*, 86(10), 1253–1264.

[19] Wang, P., Zakeeruddin, S.M., Comte, P., Charvet, R., Humphry-Baker, R. & Grätzel, M. (2003). Enhance the performance of dye-sensitized solar cells by co-grafting amphiphilic ruthenium sensitizer and hydrophobic coadsorbent. *Journal of Physical Chemistry B*, 107(48), 14336–14341.

[20] Helal, M.H., Elgemeie, G.H., El-Kashouti, M.A. & El-Zaher, A.K. (2008). Novel benzothiazapine azo dyes: Synthesis, characterization and printing properties. *Pigment & Resin Technology,* 37(1), 28–36.

[21] Zayed, M.A., Mohamed, G.G. & Fahmey, M.A. (2012). Thermal and mass spectral characterization of novel azo dyes of p-acetoamidophenol. *Journal of Thermal Analysis and Calorimetry*, 107(3), 763–776.

[22] Shalini Rosalyn, P.D., Kannan, P., Nooraldeen, A.Y., Mangayarkarasi, P.M. & Palanisamy, P.K. (2007). Azo-naphthol dyes based polymethacrylate films and their substituent effects in holography investigations. *Journal of Optoelectronics and Advanced Materials*, 9(11), 3437–3442.

[23] Chomicki, D., Kharchenko, O., Skowroński, L., Kowalonek, J., Kozanecka-Szmigiel, A., Szmigiel, D., Smokal, V., Krupka, O., & Derkowska-Zielińska, B. (2020). Physico-chemical and light-induced properties of quinoline azo-dyes polymers. *International Journal of Molecular Sciences, 21*(16), 5755. https://doi.org/10.3390/ijms21165755

[24] Karakaya, İ. (2022). Synthesis and characterization of azobenzene derived from 8-aminoquinoline in aqueous media. *Journal of the Turkish Chemical Society Section A: Chemistry*, 9(1), 85–114.

[25] Silverstein, R.M. & Webster, F.X. (2014). Spectrometric identification of organic compounds. John Wiley & Sons, Hoboken, NJ.

[26] Coates, J. (2006). Interpretation of infrared spectra, a practical approach. In: Meyers, R.A. (Ed.), Encyclopedia of Analytical Chemistry. John Wiley & Sons, Chichester, pp. 10815–10837.

[27] Khattab, T.A. (2017). Synthesis and characterization of novel azo dyes: Spectral properties and applications. *Journal of Molecular Structure*, 1134, 121–129.

[28] Hunger, K. (2003). Industrial dyes: Chemistry, properties, applications. Wiley-VCH, Weinheim.

[29] Griffiths, J. (2000). Colour and constitution of organic molecules. Academic Press, London.

[30] Robin, M. B., & Simpson, W. T. (1962). Assignment of electronic transitions in azo dye prototypes. *The Journal of Chemical Physics*, *36*(3), 580–588. https://doi.org/10.1063/1.1732574

[31] Calogero, G., Yum, J.-H., Sinopoli, A., Di Marco, G., Grätzel, M. & Nazeeruddin, M.K. (2012). Anthocyanins and betalains as natural photosensitizers for dye-sensitized solar cells. Solar Energy, 86(5), 1563–1575.